Soft Twisting Pneumatic Actuators Enabled by Freeform Surface Design

Feifei Chen, *Member, IEEE*, Yunpeng Miao, Guoying Gu, *Member, IEEE*, and Xiangyang Zhu, *Member, IEEE*

***Abstract*—Twisting motion plays an important role in kinematics of soft robots. However, current twisting actuators usually suffer from complex mechanical design with multiple materials and undesired coupling with bending and stretching motions. In this letter, we propose a new class of soft twisting pneumatic actuators that purely rely on the freeform chamber geometry to achieve large bi-directional twisting rotations. The freeform chamber surface integrates geometric flexibility in the cross section, lateral profile, and axial chirality, which are parameterized as design variables. We develop a finite element analysis model and investigate the effect of the geometry parameters on the actuators' mechanical behavior. The actuator naturally undergoes combined twisting and axial motions, and achieves a bi-directional twisting rotation of 116.7°, blocking torque of 0.81 N · m, and energy density of 1907 J/m ^{3}, well in line with the theoretical prediction. When it is constrained from axial motions, the actuator delivers pure twisting motion, achieving a bi-directional twisting rotation of 72.5°, blocking torque of 0.56 N· m, and energy density of 925 J/m^3. This letter represents an important step toward leveraging the full potential of the freeform geometry design to create novel compact soft-bodied actuators and robots.**

***Index Terms*—Soft sensors and actuators, computational geometry, soft robot materials and design.**

I. Introduction

TWISTING is a basic mode of motion and plays an essential role in flexible motion behaviors of soft robots. The analog of soft twisting actuators can be found in human wrists [1], and electric motors in conventional rigid robots. Human wrists empower hands with dexterity and contribute greatly to the manipulation capabilities of the arm/hand system [2], by flexibly orienting the end-effectors without imparting significant translational motions. In the community of soft robotics, people have well studied end-effectors such as soft hands and grippers over the past decade [3], while less attention has been paid to the development of twisting actuators.

Alike to stretching and bending, twisting of soft bodies is generated through deformation of elastic members, instead of relying on rotational joints in conventional rigid robots. This difference in the inherent mechanism has led to a fundamental shift in the design paradigm of soft actuators and robots [4]–[6]. Compared to soft bending motions that have been extensively investigated [7], soft twisting actuation is less intuitive, and the design methods are much less developed. Besides, most current soft twisting actuators rely on coupling with stretching and bending motions, making it inconvenient for control. In practical manipulation and grasping scenarios, however, pure twisting motions are usually desired. Twisting motions are combined results of complex interplay between structure and actuation. Among various actuation technologies, pneumatic actuators have been widely used for their simple configuration, low cost, and fast response [8], and thus are employed in this letter. The key to generating twisting rotation is the inclusion of rotational asymmetry into the actuator, which, in many cases, translates into the inclusion of oblique features, in an analog to spiral structures found in natural lives. For example, Kier proposed that the spiral twisting of squid tentacles along a preferred direction is due to the asymmetric orientation of fibers in their muscles [9].

In terms of generation of the oblique feature, the design strategies of soft pneumatic twisting actuators generally fall into two categories. The first approach represents a multimaterial perspective. The oblique features are typically made of stronger materials which can be paper strips [10], plastics [11], homogeneous materials [12], and fibers [13], [14]. For example, Martinez *et al.* [10] developed a pneumatic twisting actuator with a helical paper strip wrapped around a cylindrical channel. Lee *et al.* [12] combined two different materials using 3D printing techniques to build modularized twisting actuators. Connolly *et al.* [13] and Polygerinos *et al.* [14] wrapped fibers along two directions on soft tubes to program the twisting motion. Ma *et al.* presented a design framework for general soft pneumatic objects with desired motions including twisting by optimizing the multimaterial distributions [15].

The second approach relies on directly modifying the geometry of pneumatic chambers [16]–[18]. The spiral pneumatic chambers generate twisting motions upon pressurization [19]. Based on pneumatic networks [20], Wang *et al.* shifted the chamber arrangement from vertical to oblique, leading to combined bending and twisting motions [21]. Recently, Jiao *et al.*

Manuscript received October 15, 2020; accepted February 28, 2021. Date of publication April 13, 2021; date of current version April 29, 2021. This letter was recommended for publication by Associate Editor R. Niiyama and Editor K. J. Cho upon evaluation of the reviewers' comments. This work was supported in part by the National Natural Science Foundation of China under Grant 51905340, and was sponsored by Shanghai Sailing Program under Grant 19YF1422900. *(Corresponding author: Feifei Chen.)*

The authors are with the State Key Laboratory of Mechanical System and Vibration, Shanghai Jiao Tong University and Robotics Institute, School of Mechanical Engineering, Shanghai Jiao Tong University, Shanghai 200240, China (e-mail: ffchen@sjtu.edu.cn; mythmyp@sjtu.edu.cn; guguoying@sjtu.edu.cn; mexyzhu@sjtu.edu.cn).

This letter has supplementary downloadable material available at https://doi.org/10.1109/LRA.2021.3072813, provided by the authors.

Digital Object Identifier 10.1109/LRA.2021.3072813

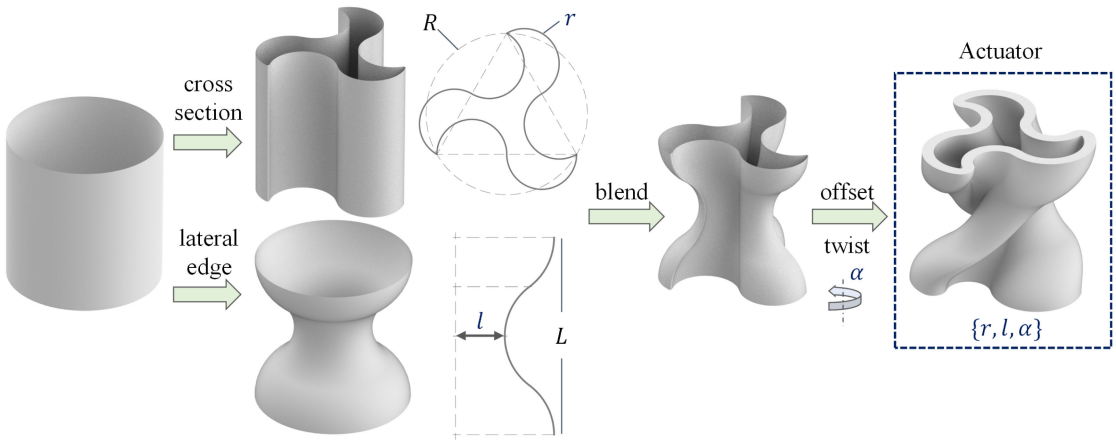

Fig. 1. The geometry generation process of the twisting actuator.

demonstrated vacuum-powered twisting actuators by pre-twisting the chambers, and pure torsions can be produced by connecting two twisting units to cancel out the stretching motion [22]. Besides, Yang *et al.* proposed a new deformation strategy of soft actuators through buckling of simple chambers [23]. When vacuumized, the chambers' beams would buckle and induce local planar rotation and global contraction. Lazarus *et al.* introduced patterned voids into soft tubes to achieve twisting motions upon distributed actuations [24].

Geometry-based design approach has advantages over the multimaterial approach since it only relies on the chamber shape and thus requires a single material, leading to less fabrication complexity and cost. Geometry plays a central role in defining the mechanical behavior, but it has been less investigated especially in soft pneumatic actuators due to the difficulty caused by the complex interplay between geometry and actuation such as the design-dependency of the pressure loading [6]. To date, it is still an open question how freeform geometry design in a general sense can deliver desired motion behaviors such as twisting. The aforementioned works usually consider only one aspect of geometric features at the design stage, resulting in relatively small design space. An absolutely general geometry model is impractical, but instead it must be parameterized. To this end, the selection and representation of key geometry features that have main impact on the concerned mechanical behaviors become very important.

In this paper, from a perspective of geometry design, we propose a new type of soft pneumatic twisting actuators with advantages of large-stroke twisting rotation, by exploiting the freeform surface of the actuator chamber. The geometry model should be hierarchical to capture global and local features, and in this letter we focus on the first level, i.e., the key global features that dominate the actuator's twisting behavior. We present a parametric freeform chamber geometry that integrates three key features as design variables: the cross section, lateral profile, and axial chirality, as shown in Fig. 1. The three geometric parameters span a set of shapes, i.e. the design space.

To explore the design space for desired twisting behaviors, we develop a nonlinear finite element analysis model and write python scripts to automate the process of performance evaluation of the design candidates. Compared with previous works that mainly focused on the twisting motions only, we further investigate the load capability by evaluating the blocking torque, which is important for practical use in soft robotic systems. In consideration of both motion and load capabilities, we prototype the optimal design with the largest energy density, and a free twisting rotation of 116.7° (positive 85.3° and negative 31.4°), blocking torque of 0.81 N · m, and energy density of 1907 J/m^3 are achieved, which agree well with the theoretical prediction and outperform existing twisting actuators.

Another significant concern is the function of producing pure twisting motions. In previous works, the twisting motions are typically coupled with stretching, compression, or bending, which is undesired in many practical scenarios. Here, we show that, when the actuator is constrained from axial motion by embedding a rigid axle inside, it can deliver pure torsions, with the maximal twisting rotation of 72.5° (positive 59.0° and negative 13.5°), blocking torque 0.56 N · m, and energy density 925 J/m^3. To our best knowledge, this is the first report and quantitative investigation of soft pneumatic actuators that purely twist.

This letter represents an initial step toward leveraging the full potential of the freeform geometry design to create novel compact soft-bodied actuators. The geometric characteristics of the soft body work in concert to produce the desired twisting motions and this design paradigm purely relying on freeform surface is especially attractive for applications which require compact-sized body and convenient fabrication. Benefiting from the single-material design, the actuator can be readily fabricated using the mature molding and casting process and it exhibits excellent stability, reliability, and long lifetime. In a more general sense, the freeform design can be further developed, in combination with topology optimization theory [6], [25], [26] and conformal geometry theory [27], [28], to directly encode desired complex behaviors in the body shape of soft robots.

II. Geometry Design

The geometry design of our proposed twisting actuator can be taken as a transformer from a cylindrical tube of outer radius

R and height L, by undergoing the following three steps, as shown in Fig. 1. First, the cross section is switched from a circle to a rotational symmetric geometry, and we adopt a horseshoe shape that is often used in metamaterial design as in [29], [30], with the arc radius denoted by r. Numerical studies show that the triangular horseshoe shape typically delivers larger twisting motions than other polygonal counterparts, and thus is selected in the design. Second, the lateral profile is changed to be concave like a classical bellow-type actuator which helps attain larger stretchability along the longitudinal direction and well avoid the ballooning effect in the radial direction. Specifically, the lateral edge consists of three tangential arcs with the same radius determined by the minimal distance relative to the center axis, denoted by l. Third, the end-face is pre-twisted relative to the other by an angle α. The freeform surface of the actuator well integrates these three features by a linear blending operation. A large family of freeform surfaces can be generated by modulating the geometry features which span a large design space to be explored.

To facilitate design exploration, the parameterization of the freeform surface is necessary. We fix the parameters: $L = 40\,\mathrm{mm}$, and $R = 20\,\mathrm{mm}$. In this way, the actuator geometry can be fully described by only three parameters: $\{r, l, \alpha\}$. As shown in the supplementary video, we write a Rhino script to generate the CAD model with prescribed parameters automatically. First, the script creates a group of horseshoe-shaped cross sections with the maximal radii scaled by the bellow-type lateral edge. Then, these curves are merged by lofting to generate an integral smooth surface. Thereafter, the surface is offset by a fixed thickness $t = 3\,\mathrm{mm}$ to create a solid part. Last, we apply twisting on the solid part along the center axis and export it as an STP file to be submitted to Abaqus for analysis.

III. Simulation-Driven Design Exploration

In this section, we will conduct nonlinear finite element analysis to study the effect of the geometric parameters on the resulting mechanical behavior of the actuator, and thus to produce the desired performance in terms of the twisting motion and output torque.

A. Material Characterization

To sustain large stroke, the material to fabricate the soft actuator should be highly deformable and exhibit good hyperelasticity. Without loss of generality, we employ the Neo-Hookean model [31], to characterize the hyperelasticity. The deformation gradient is defined as $\vec{F} = \vec{I} + \nabla\vec{u}$ with $\vec{u}$ the displacement field. The strain energy density function is described by $W = \frac{\mu}{2}(I_1 - 3)$ where μ is the shear modulus and I_1 is the first invariant of Cauchy-Green deformation tensor, i.e., $I_1 = \mathrm{trace}(\vec{F}^{\mathrm{T}}\vec{F})$.

Based on some preliminary tests, we selected a type of polyurethane-based silicone rubber Hei-Cast 8400 as the material, and the standard specimens according to ASTM E8 were tested by uniaxial tension experiments. The specimens each were stretched at a fixed rate of 300 mm/min by the tensile tester (Zwick Roell Z100), until 3.5 times its original length. Based on the experimental results of the force-displacement relation, we obtained the nominal stress and strain data. We denote the stretch ratio of the lengthwise direction by λ, and the stretch ratios of the other two orthogonal directions in the cross-section of the samples are $1/\sqrt{\lambda}$, with the assumption that the polyurethane is incompressible. Based on the strain energy density, the nominal stress σ is related to the stretch ratio by

$$\sigma = \mu\left(\lambda - \frac{1}{\lambda^2}\right). \tag{1}$$

The derivation details can be found in [32]. We then fit the material model with uniaxial tensile test data using MatEditor (WELSIM) fitting procedure, and the shear modulus of Hei-Cast 8400 is 0.34 MPa.

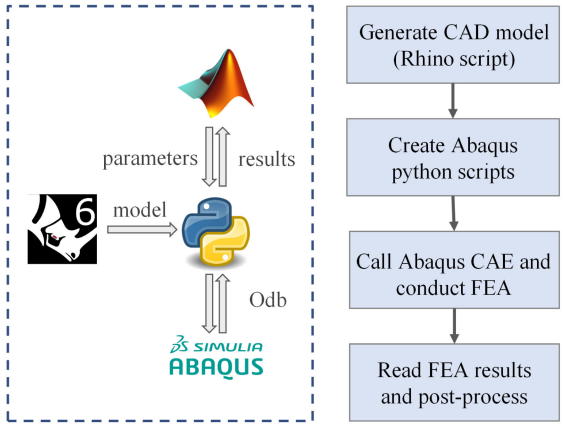

Fig. 2. The whole workflow of the simulation framework.

B. Nonlinear Finite Element Analysis

To automate the evaluation of the actuator design candidate, we develop a simulation framework. As shown in Fig. 2, we connect Matlab, Abaqus, and Rhino with python scripts. In this framework, the geometric parameters $\{r, l, \alpha\}$ are varied in Matlab and encoded in python scripts. Then, Rhino scripts are used to generate the CAD model corresponding to the parameters. Thereafter, Matlab invokes Abaqus (no GUI) to perform the finite element analysis that incorporates both geometric and material nonlinearities, by automatically running python scripts. Finally, the results of displacements and reaction torques are read by Matlab and the simulation iterates by repeating the steps above.

Here we demonstrate an example to elaborate the finite element analysis, with the geometric parameters $r = 5\sqrt{3}$ mm, $l = 10$ mm, and $\alpha = 60°$. We use C3D4H elements (4-node linear tetrahedron and hybrid) to mesh the CAD model, as shown in Fig. 3(a). The twisting angle θ and output torque τ are the two most important performance indicators of the actuator. To attain the maximal twisting angle, the actuator is fixed at one end with the other end moving freely in space. In Abaqus, the bottom plane is encastred and the top plane is coupled with a reference point to act as a rigid plate. As shown in Fig. 3(b), the actuator twists remarkably with the applied pressure, and the maximal stress occurs on highly curved regions of the inner surface.

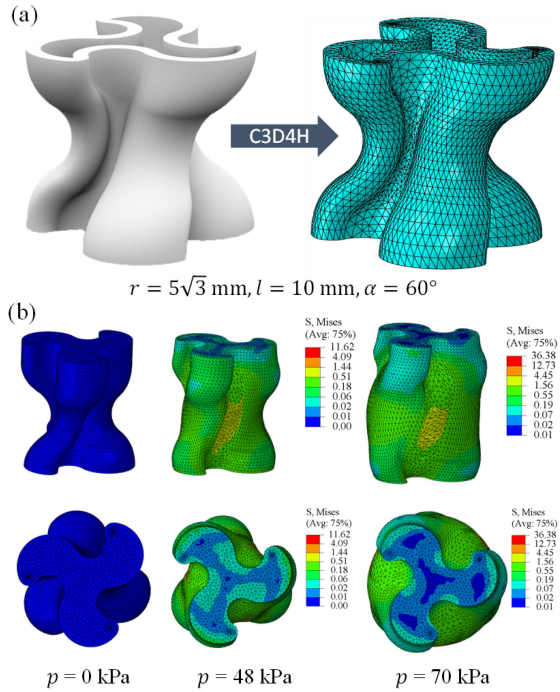

Fig. 3. (a) The CAD model and the mesh (C3D4H); (b) the states of twisting rotations under different pressure, with $r = 5\sqrt{3}$ mm, $l = 10$ mm, and $\alpha = 60°$.

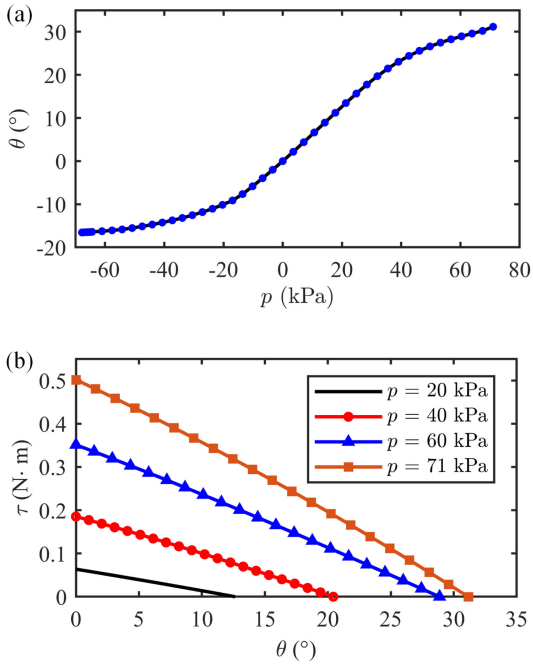

Fig. 4. (a) The free twisting rotation and (b) the torque-rotation curves of the actuator under different pressure, with $r = 5\sqrt{3}$ mm, $l = 10$ mm, and $\alpha = 60°$.

When the pressure is negative, the actuator twists along the opposite direction. The actuator experiences combined motions of axial elongation/compression and twisting, and no bending is involved. As shown in Fig. 4(a), the twisting angle changes from -18° to 31° when the applied pressure varies from -68 kPa to 71 kPa.

TABLE I
PARAMETER SETTING FOR DESIGN EXPLORATION

Variable	Physical significance	Range	Step
r	cross section shape	$5\sqrt{3}$ mm $\sim$ 20 mm	0.5 mm
l	lateral profile	10 mm $\sim$ 20 mm	1 mm
α	pre-twisting angle	60° $\sim$ 360°	2°

To evaluate the actuator's load capability, the blocking torque is investigated by constraining the actuator from rotation and the reactive torque is recorded. Fig. 4(b) shows the torque-rotation relation at different pressures, and the blocking torque is identified as the maximal torque when the rotation is fully constrained. It is observed that the torque-rotation relation exhibits excellent linearity for different levels of pressure loading. This linearity is also verified on some randomly selected design parameters. Thus, the torque-rotation relation of the actuators in the design space can be fully characterized by the free twisting rotation and blocking torque, with which we may readily calculate the maximal energy density denoted by Ω as follows

$$\Omega = \frac{\tau\theta}{8\,V} \tag{2}$$

The volume V here is defined as the maximal space the actuator may occupy instead of volume of the material usage, i.e. $V = \pi R_0^2\, L$ where $R_0 = 25\,\mathrm{mm}$ is the maximal radius of the actuator.

C. Design Exploration

Further, we investigate the effect of the geometric parameters on the resulting deformation behavior of the actuator. The ranges and variation steps of the parameters are listed in Table I. Fig. 5 shows the finite element analysis results of free motion and blocking torque. For clarity of presentation, only three representative values of the arc radius in the cross section are displayed, i.e. $r = 5\sqrt{3}$ mm, 13.2 mm, 20 mm. In each simulation case, the applied pressure keeps being increased until the analysis fails, typically due to the mesh distortion when the ballooning effect in the radial direction occurs. By combining the results of free motion and blocking torque, we are able to calculate the energy density based on Eq. (2) under the same pressure which is selected to be the lower one from the two cases of free motion and blocking torque.

1) Free Motion: The maximal twisting rotation angle and its corresponding pressure for each investigated design candidate are plotted in Fig. 5(a). We observe a general trend that the twisting rotation θ increases with the pre-twisting angle α and the arc curvature in the cross section $1/r$. The lateral profile described by l has a marginal effect on the twisting angle, while it mainly controls the radial expansion. Because one does not expect overt ballooning effects, the maximal radius after deformation is restricted to be $1.15R_0$, and the design candidates resulting in larger expansion are abandoned. As shown in Fig. 5, the plots are divided into two parts: feasible designs highlighted by the colorful region and the infeasible designs highlighted by the gray region. Among the feasible solutions, the maximal free twisting angle is 172.3°, and the corresponding parameters are $r = 5\sqrt{3}$ mm, $l = 11.75$ mm, $\alpha = 360°$, and $p = 39.98$ kPa.

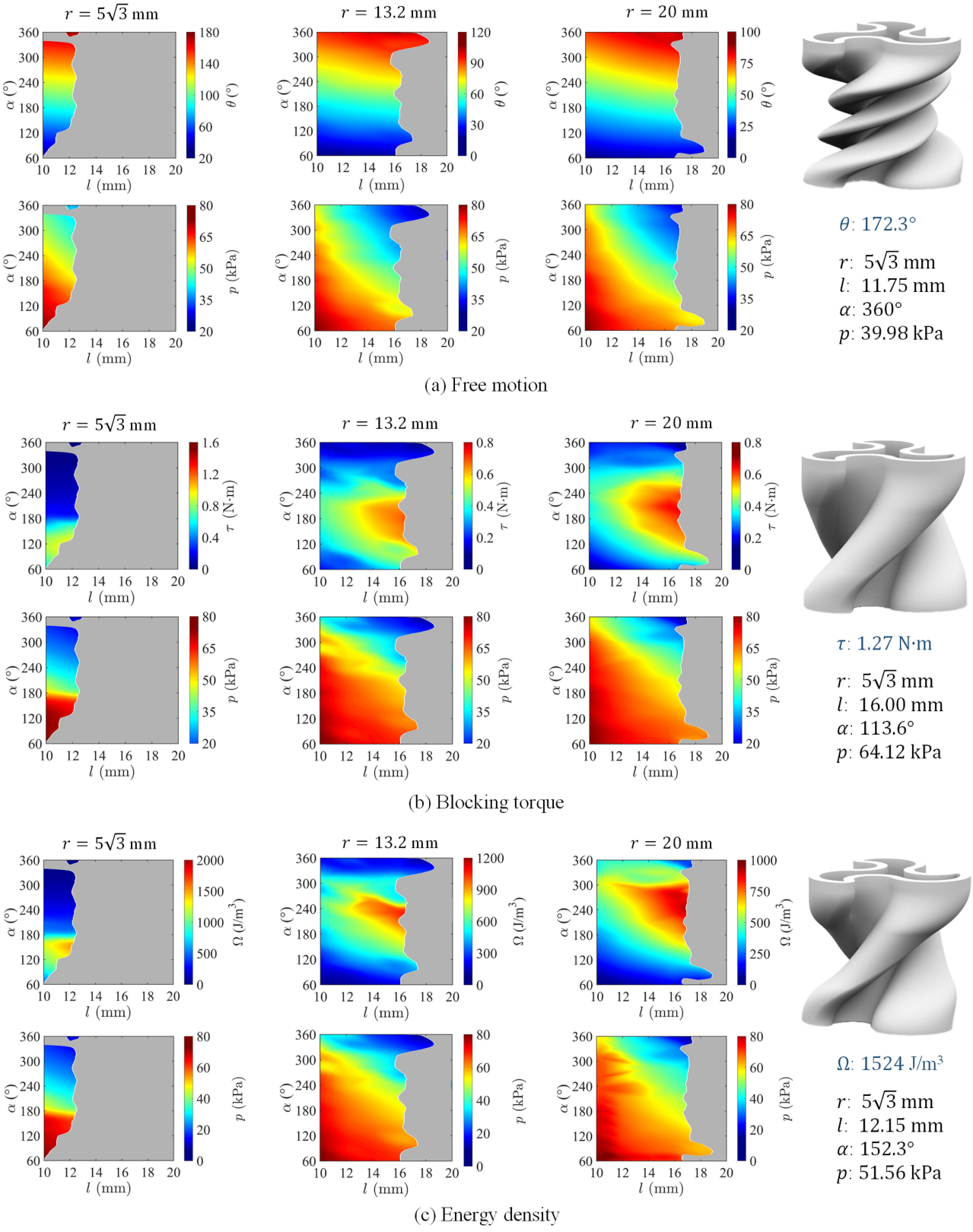

Fig. 5. Simulation-driven design exploration of the actuator.

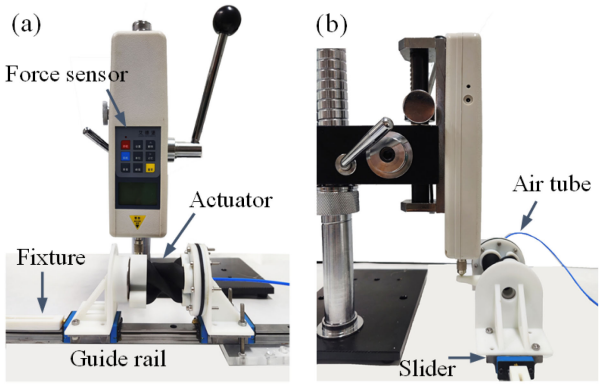

Fig. 6. The experiment setup.

2) Blocking Torque: The blocking torque and its corresponding pressure for each design candidate are plotted in Fig. 5(b). It is generally observed that the blocking torque τ initially increases with the pre-twisting angle α, peaks at a critical point which depends on the values of r and l, and then decreases. The critical point is identified as the optimal pre-twisting angle, which increases with the arc radius r. It can be concluded that a larger pre-twisting angle leads to a larger free twisting rotation but not necessarily a larger blocking torque, due to the low stiffness when the actuator is highly pre-twisted. When the lateral edge becomes flat (larger l), the blocking torque increases accordingly but the ballooning effect becomes more pronounced in the meantime. In the feasible solutions, the maximal blocking torque is 1.27 N $\cdot$ m, and the corresponding parameters are $r = 5\sqrt{3}$ mm, $l = 16.00$ mm, $\alpha = 113.6^\circ$, and $p = 64.12$ kPa.

3) Energy Density: The energy densities are calculated based on the results of free motion and blocking torque, and the results are shown in Fig. 5(c). When the geometric parameters are $r = 5\sqrt{3}$ mm, $l = 12.15$ mm, $\alpha = 152.3^\circ$, and $p = 51.56$ kPa, the actuator attains a free twisting angle of 79.8° and blocking torque 0.69 N $\cdot$ m, resulting in the maximal energy density 1524 J/m^3. The physical significance of energy density is the maximal work the actuator can perform. Hence, we select the design with the optimal energy density and prototype it for experimental validation.

IV. Experiment

A. Setup

The actuator is prototyped by a molding and casting process using Hei-Cast 8400. In order to measure the twisting angle and blocking torque, a test platform is set up as shown in Fig. 6. We first install the actuator with rigid caps and fasten one end on the slider with bolts. A flange with a lever is connected to the top of the actuator and is held by a bearing fixed on another slider. After that, sliders are installed onto the guide rail (LWE15; IKO). To allow the test for pure torsions, a fixture is fabricated to limit the axial motion. The twisting motion of the actuator is captured by a 3D tracking system (OptiTrack PRIME 13; NaturalPoint), and the twisting angle is measured by two markers attached to the top plate as connected by the red line in Fig. 7(a). The blocking torque is calculated based on the blocking force measured by the force sensor (HP200, $\pm 0 \sim 200$ N; HANDPI) and its arm 50 mm. All fixtures are fabricated with VeroWhitePure by 3D printing using PolyJet J750 (Stratasys).

A customized pneumatic control system is constructed to power the actuator. The pressurized air is produced by an air compressor (2X950-50; OUTSTANDING), and the range of the output pressure is -93 kPa $\sim$ 500 kPa. To regulate the pressure loading path, we code Matlab Simulink programs and use dSpace (DS1202; dSPACE GmbH) to control the output pressure. A barometer (AZ9631, $\pm 0 \sim 689.5$ kPa; AZ Instrument Corp.) is used to monitor the applied pressure.

B. Performance Characterization

We characterize the performance of the actuator firstly when it undergoes combined twisting and axial motions, and subsequently when it experiences pure torsions, both under a wide range of pressurization including positive and negative pressures. Fig. 7(a) shows the reference and deformed states of the actuator. It is observed that, before the obvious ballooning phenomenon occurs, remarkably large twisting motions are obtained, i.e. 85.3° and -29.5° for combined twisting and 59.0° and -11.9° for pure twisting. To enable pure twisting, a rigid axle is embedded inside the actuator to constrain the axial motion.

Fig. 7(b) shows the results of free motion in the cases of both combined and pure torsions, and the experiment results agree well with the simulation. In simulation for negative pressure, we define perfect contact constraints between parts of the actuator and the lower limit of pressure approaches vacuuming. It is observed that the twisting angle increases with the applied pressure monotonically and smoothly. Positive pressure loading results in a wider range of motion. Specifically, the rotation angle increases almost linearly with the pressure, and grow slowly at a high level of pressure loading when the radial ballooning effect dominates. In this test and what follows, five identical actuator prototypes are evaluated at their average values on three trials for each experiment, with the error bar plotted as shown in Figs. 7(b) and (c). The narrow error bars indicate that the prototypes exhibit high consistency.

Fig. 7(c) shows that the blocking torque increases with the applied pressure over a large range, even when the radial expansion dominates at high pressures. It is also found that the load capability under negative pressure is limited, well in line with the theoretical prediction. Based on the free motion and blocking torque results, we obtain the experimental energy densities as shown in Fig. 8, which reach as large as 1906.9 J/m^3 and 925.2 J/m^3 in the modes of combined twisting and pure twisting, respectively. The overall performance of the actuator is summarized in Table II.

We further evaluate the dynamic performance of the actuator by applying step signals and found that the actuator responds quickly (less than 0.1 s), as shown in the supplementary video, due to the low viscosity of the material. Further, to test the stability and durability of the actuator, we apply a cyclic pressure loading with frequency 0.5 Hz to run over 25 000 cycles and no material failure or performance attenuation is found. We demonstrate a straightforward application in which the actuator assembled with a one-way bearing can unscrew a tight bottle cap

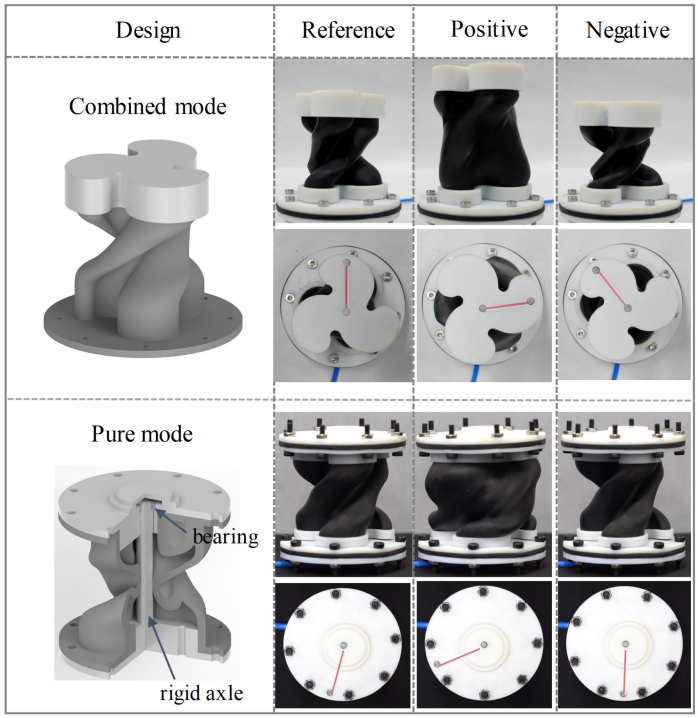

(a) The experimental states of the actuator in free motion

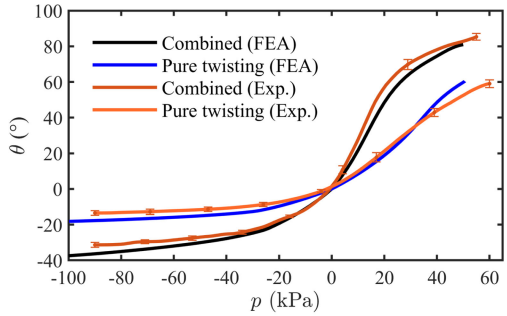

(b) The experimental result of free motion

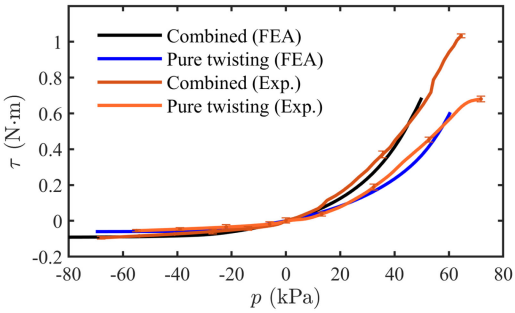

(c) The experimental result of blocking torque

Fig. 7. The performance of the actuator in combined mode and pure twisting mode.

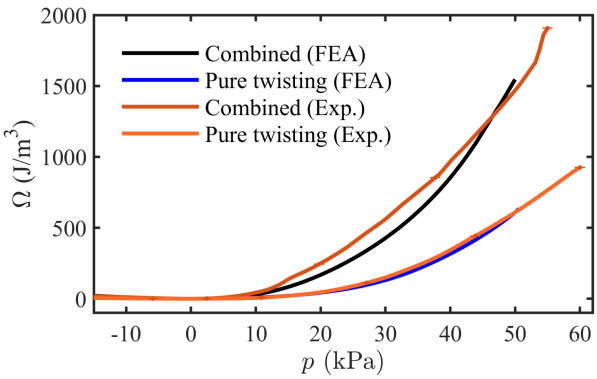

Fig. 8. The experimental result of energy density.

TABLE II
EXPERIMENTAL PERFORMANCE OF ACTUATOR PROTOTYPE

		Twisting Rotation (°)	Blocking Torque (N·m)	Energy Density (J/m³)
Combined	positive p	85.3	0.81	1906.9
	negative p	−29.5	−0.10	77.5
Pure Twisting	positive p	59.0	0.56	925.2
	negative p	−11.9	−0.06	18.2

by repeatedly twisting. The actuator is also promising for use in wrist-like manipulation and locomotion. It has been observed from animals that the spine's twisting motion plays an important role in legged locomotion by controlling the body's swing and gaits [33]. Our designed twisting actuator can be readily integrated into soft robotic systems to assist in locomotion.

TABLE III
COMPARISON BETWEEN OUR WORK AND OTHER TWISTING ACTUATORS IN LITERATURE

	θ (°)	θ/L (°/mm)	τ (N·m)	V (mm³)	M (g)	Ω (J/m³)	Ω_M (J/kg)
Sanan 2014 [17]	60.0	0.3	66	1 178 097	-	7333.3	-
Connolly 2015 [13]	200.0	1.2	-	36 142	-	-	-
Lazarus 2015 [24]	63.0	0.7	-	195 571	-	-	-
Yang 2015 [23]	30.0	1.5	-	8000	9.0	-	-
Yan 2018 [18]	110.0	2.2	0.026	12 723	-	490.4	-
Jiao 2019 [22]	120.0	2.0	0.225	64 000	19.0	920.4	3.10
Darekar [19]	45.4	0.5	0.69	855 299	-	222.4	-
Our work	85.3	2.1	0.810	78 540	29.0	1906.9	5.20

C. Discussion

As validated by the simulation and experiment, the freeform surface design of the actuator has led to the remarkable performance in terms of the twisting motion and load capability. As shown in Table III, we compare our actuator with some other twisting actuators reported in literature recently. The energy densities in terms of volume (denoted by Ω) and mass (denoted by Ω_M) are calculated for comparison, based on the data provided in the referred works. It is found that the proposed design attains good performance in terms of the twisting angle per length and energy density.

The geometry design approach in this letter also saves fabrication complexity and leads to better performance. Since the

twisting motion is fully generated by virtue of the freeform surface, one is allowed to fabricate the actuator using a single material, with the mature molding and casting techniques. In comparison with the twisting design based on 3D printed multi-materials [12] that may easily suffer from material failures [34], the single-material design fabricated by casting in this letter attains better performance in terms of the material stretchability, viscoelasticity, and resilience.

The present work also has limitations. With three geometry parameters only, the design paradigm deals with a limited set of shapes. In a general sense, the geometry model should be hierarchical to capture global and local features, and in this letter we focus on the first level, i.e., the key global features that dominate the actuator's twisting behavior. Each geometry feature can be further parameterized and refined. Further investigation of the geometry parameters on the level of single feature is worth research endeavor and will definitely improve the design. With the increase of design parameters, full exploration will be impractical, but instead optimization algorithms should be developed, which will be included in our future work.

V. Conclusion

In this letter, we provide a novel class of twisting actuators by harnessing freeform surface design of the air chamber, which can achieve bi-directional twisting motions of 72.5° and 116.7 °, and blocking torque of 0.56 N · m and 0.81 N · m, in the combined motion mode and pure twisting mode, respectively. The freeform chamber surface is generated by combining the geometric flexibility in the cross section, lateral profile, and pre-twisting angle, and it is parameterized using three parameters for design optimization. The complex interplay among the geometric parameters and the pressure loading is addressed by the nonlinear finite element analysis. The parametric geometry design approach leads to a compact-sized body of the actuator consisting of a single material.

References

[1] N. M. Bajaj, A. J. Spiers, and A. M. Dollar, "State of the art in artificial wrists: A review of prosthetic and robotic wrist design," *IEEE Trans. Robot.*, vol. 35, no. 1, pp. 261–277, Feb. 2019.

[2] F. Montagnani, M. Controzzi, and C. Cipriani, "Is it finger or wrist dexterity that is missing in current hand prostheses?," *IEEE Trans. Neural Syst. Rehabil. Eng.*, vol. 23, no. 4, pp. 600–609, Jul. 2015.

[3] Z. Shen, F. Chen, X. Zhu, K.-T. Yong, and G. Gu, "Stimuli-responsive functional materials for soft robotics," *J. Mater. Chem. B*, vol. 8, no. 39, pp. 8972–8991, 2020.

[4] F. Chen, K. Liu, Y. Wang, J. Zou, G. Gu, and X. Zhu, "Automatic design of soft dielectric elastomer actuators with optimal spatial electric fields," *IEEE Trans. Robot.*, vol. 35, no. 5, pp. 1150–1165, Oct. 2019.

[5] F. Chen *et al.*, "Topology optimized design, fabrication, and characterization of a soft cable-driven gripper," *IEEE Robot. Automat. Lett.*, vol. 3, no. 3, pp. 2463–2470, Jul. 2018.

[6] F. Chen and M. Y. Wang, "Design optimization of soft robots: A review of the state of the art," *IEEE Robot. Automat. Mag.*, vol. 27, no. 4, pp. 27–43, Dec. 2020.

[7] Q. Pan, S. Chen, F. Chen, and X. Zhu, "Programmable soft bending actuators with auxetic metamaterials," *Sci. China Technological Sci.*, vol. 63, no. 12, pp. 2518–2526, 2020.

[8] F. Ilievski, A. D. Mazzeo, R. F. Shepherd, X. Chen, and G. M. Whitesides, "Soft robotics for chemists," *Angewandte Chemie*, vol. 123, no. 8, pp. 1930–1935, 2011.

[9] W. M. Kier, "The musculature of squid arms and tentacles: Ultrastructural evidence for functional differences," *J. Morphol.*, vol. 185, no. 2, pp. 223–239, 1985.

[10] R. V. Martinez, C. R. Fish, X. Chen, and G. M. Whitesides, "Elastomeric origami: Programmable paper-elastomer composites as pneumatic actuators," *Adv. Funct. Mater.*, vol. 22, no. 7, pp. 1376–1384, Apr. 2012.

[11] L. Belding *et al.*, "Slit tubes for semisoft pneumatic actuators," *Adv. Mater.*, vol. 30, no. 9, Mar. 2018, Art. no. 1704446.

[12] J.-Y. Lee, W.-B. Kim, W.-Y. Choi, and K.-J. Cho, "Soft robotic blocks: Introducing SoBL, a fast-build modularized design block," *IEEE Robot. Automat. Mag.*, vol. 23, no. 3, pp. 30–41, Sep. 2016.

[13] F. Connolly, P. Polygerinos, C. J. Walsh, and K. Bertoldi, "Mechanical programming of soft actuators by varying fiber angle," *Soft Robot.*, vol. 2, no. 1, pp. 26–32, 2015.

[14] P. Polygerinos *et al.*, "Modeling of soft fiber-reinforced bending actuators," *IEEE Trans. Robot.*, vol. 31, no. 3, pp. 778–789, Jun. 2015.

[15] L.-K. Ma, Y. Zhang, Y. Liu, K. Zhou, and X. Tong, "Computational design and fabrication of soft pneumatic objects with desired deformations," *ACM Trans. Graph.*, vol. 36, no. 6, pp. 1–12, 2017.

[16] B. Gorissen, T. Chishiro, S. Shimomura, D. Reynaerts, M. De Volder, and S. Konishi, "Flexible pneumatic twisting actuators and their application to tilting micromirrors," *Sensors Actuators A: Phys.*, vol. 216, pp. 426–431, 2014.

[17] S. Sanan, P. S. Lynn, and S. T. Griffith, "Pneumatic torsional actuators for inflatable robots," *J. Mechanisms Robot.*, vol. 6, no. 3, 2014, Art no. 0 31003.

[18] J. Yan, X. Zhang, B. Xu, and J. Zhao, "A new spiral-type inflatable pure torsional soft actuator," *Soft Robot.*, vol. 5, no. 5, pp. 527–540, 2018.

[19] B. Darekar, "Development of multi-chamber pneumatic twist actuator for soft robot," 2018, Accessed: Dec. 30, 2020. [Online]. Available: https://bhushandarekar.com/project/development-of-multi-chamber-pneumatic-twist-actuator-for-soft-robot

[20] B. Mosadegh *et al.*, "Pneumatic networks for soft robotics that actuate rapidly," *Adv. Funct. Mater.*, vol. 24, no. 15, pp. 2163–2170, 2014.

[21] T. Wang, L. Ge, and G. Gu, "Programmable design of soft pneu-net actuators with oblique chambers can generate coupled bending and twisting motions," *Sensors Actuators A: Phys.*, vol. 271, pp. 131–138, 2018.

[22] Z. Jiao, C. Ji, J. Zou, H. Yang, and M. Pan, "Vacuum-powered soft pneumatic twisting actuators to empower new capabilities for soft robots," *Adv. Mater. Technol.*, vol. 4, no. 1, Jan. 2019, Art no. 1800429.

[23] D. Yang *et al.*, "Buckling of elastomeric beams enables actuation of soft machines," *Adv. Mater.*, vol. 27, no. 41, pp. 6323–6327, Nov. 2015.

[24] A. Lazarus and P. M. Reis, "Soft actuation of structured cylinders through auxetic behavior," *Adv. Eng. Mater.*, vol. 17, no. 6, pp. 815–820, 2015.

[25] M. Y. Wang, X. Wang, and D. Guo, "A level set method for structural topology optimization," *Comput. Methods Appl. Mechanics Eng.*, vol. 192, no. 1, pp. 227–246, 2003.

[26] F. Chen, Y. Wang, M. Y. Wang, and Y. Zhang, "Topology optimization of hyperelastic structures using a level set method," *J. Comput. Phys.*, vol. 351, pp. 437–454, 2017.

[27] S. Wang, Y. Wang, M. Jin, X. D. Gu, and D. Samaras, "Conformal geometry and its applications on 3D shape matching, recognition, and stitching," *IEEE Trans. Pattern Anal. Mach. Intell.*, vol. 29, no. 7, pp. 1209–1220, Jul. 2007.

[28] Q. Ye, Y. Guo, S. Chen, N. Lei, and X. D. Gu, "Topology optimization of conformal structures on manifolds using extended level set methods (x-lsm) and conformal geometry theory," *Comput. Methods Appl. Mechanics Eng.*, vol. 344, pp. 164–185, 2019.

[29] K.-I. Jang *et al.*, "Soft network composite materials with deterministic and bio-inspired designs," *Nature Commun.*, vol. 6, no. 1, pp. 1–11, 2015.

[30] Q. Ma *et al.*, "A nonlinear mechanics model of bio-inspired hierarchical lattice materials consisting of horseshoe microstructures," *J. Mechanics Phys. Solids*, vol. 90, pp. 179–202, 2016.

[31] R. Rivlin, "Large elastic deformations of isotropic materials iv. further developments of the general theory," *Philos. Trans. Roy. Soc. London. Ser. A., Math. Phys. Sci.*, vol. 241, no. 835, pp. 379–397, 1948.

[32] R. W. Ogden, *Non-Linear Elastic Deformations*. Courier Corporation, Apr. 2013.

[33] J. C. Case, J. Gibert, J. Booth, V. SunSpiral, and R. Kramer-Bottiglio, "Spinal helical actuation patterns for locomotion in soft robots," *IEEE Robot. Automat. Lett.*, vol. 5, no. 3, pp. 3814–3821, Jul. 2020.

[34] G. Dammer, S. Gablenz, A. Hildebrandt, and Z. Major, "Design and shape optimization of PolyJet bellows actuators," in *Proc. IEEE Int. Conf. Soft Robot. (RoboSoft)*, Apr. 2018, pp. 282–287.